TISSUE ENGINEERING: Part A
Volume 00, Number 00, 2019

DOI: 10.1089/ten.tea.2019.0209

termis
Tissue Engineering
& Regenerative Medicine
International Society

Design and Fabrication of an Automatable, 3D Printed Perfusion Device for Tissue Infusion and Perfusion Engineering

Benjamin K. Schilling, MS,[1] Kimberly K. Lamberti, BS,[2] Malik J. Snowden, BS,[1] Jocelyn S. Baker,[1] Kristen Byrd, BS,[1] Chiaki Komatsu, MD,[2] Mario G. Solari, MD,[2] and Kacey G. Marra, PhD[1–3]

Tissue decellularization for generating extracellular matrices has become a staple of regenerative medicine in the recent decades, extending from the research setting to clinical usage. Although methods and protocols for tissue decellularization are abundant throughout the literature, they can be time intensive and typically require specific overhead in terms of equipment. To reduce these barriers to entry, a functional and reproducible prototype of a tissue infusion/perfusion device (TIPD) has been designed and fabricated using three-dimensional printed parts in conjunction with commercially available components. This TIPD forms a system composed of two peristaltic pumps, two 3-way valves, and a chamber in which tissue is contained, and is controlled by user-customizable software. To increase repeatability among decellularization protocols, an automation function has been integrated into the software, which is able to specify fluid flow rates and define specific valve locations enabling selection of solutions to be introduced into a scaffold over the course of a decellularization process. The prototype has been tested for proof of concept through infusion and perfusion decellularization of skeletal muscle and intact kidneys, respectively, and has shown successful removal of cellular content while maintaining an intact ultrastructure. In an effort to increase the reproducibility of experimental designs and to promote an open source hardware initiative in the field of tissue engineering, a novel device was conceptualized and prototyped with printable part files made available for its fabrication in tandem with instructions for assembly.

Keywords: fused filament fabrication, bioreactor, open source hardware, decellularization, extracellular matrix

Impact Statement

Repeatable methods for decellularization are essential for achieving consistent substrates between batches, laboratories, and facilities. To meet this end, an automatable tissue infusion/perfusion device composed of three-dimensional printed parts and commercially available components has been prototyped and tested. Materials and instructions for its assembly have been made available in an effort to reduce variability among equipment as well as to provide a platform on which to iterate open-source hardware in tissue engineering.

Introduction

Extracellular matrices (ECMs) resulting from decellularized tissue have shown exceptional promise for repair and regeneration of damaged tissue. To that end, over 40 ECM-based products are registered, cleared, or approved for clinical use by the Food and Drug Administration in the U.S. alone.[1] Typically used for repair of homologous tissue, allogeneic and xenogeneic decellularized ECMs span a plethora of therapeutic applications. Such applications include hernia repair,[2,3] breast reconstruction,[4,5] adipose regeneration,[6] dental and orthopedic bone void repair,[7,8] tendon reconstruction,[9] and wound care.[10,11] Decellularized ECM therapies continue to be investigated through clinical trials, addressing a multitude of application anatomic sites, including the trachea, heart valves, eye, and bladder among

Departments of [1]Bioengineering and [2]Plastic Surgery, University of Pittsburgh, Pittsburgh, Pennsylvania.
[3]McGowan Institute of Regenerative Medicine, Pittsburgh, Pennsylvania.

many others.[12] Furthermore, complex structural ECM scaffolds generated from perfusion decellularization, such as heart,[13,14] lung,[15] kidney,[16] or face,[17] are within the foreseeable pipeline for future clinical translation.

While methods for tissue decellularization are abundant and reliable, these methods can also be laborious and time intensive. A given process for rendering a decellularized ECM typically contains multiple surfactants, disinfectants, and/or antibiotics, along with rinsing solution exchanges; this process must be designed to yield a material that will promote cell attachment and growth, is noncytotoxic, and will prospectively meet clinical standards.[18] Perfusion decellularization for whole organ engineering requires additional hardware that spinner flask or agitation decellularization does not, as well as similar, if not greater, requirements for solution exposure.[19]

Initial attempts at automating decellularization processes have resulted in shorter decellularization periods with greater efficiency in removing DNA material; however, automation systems are often developed for a target tissue or organ and typically include several large, piecemeal components that limit or rotation of the two chamber types prevent mobility.[20] In this study, a functional prototype of an integrated tissue infusion/perfusion device (TIPD) has been designed and fabricated using three-dimensional (3D) printed parts coupled with commercially available components. This device has been tested for proof of concept through infusion decellularization of porcine skeletal muscle and perfusion decellularization of an intact rodent kidney. In this study, the 3D-printable components, software, and circuitry files have been made available along with the instructions for the device's assembly. From these, it is our intention to decrease the burden of entry into infusion or perfusion decellularization, increase the reproducibility of experimental designs, and to promote an open-source hardware (OSH) initiative in tissue engineering.

Materials and Methods

There were several target considerations in designing the TIPD: namely these design constraints included the integration of 3D printable scaffolding coupled with the use of off-the-shelf OSH components intended to maximize flexibility for parts replacement. For purposes of mobility, the total volume of the device was to be kept under 1 cubic foot. For fluidics, the integration of programmatic control at two peristaltic pumps (to govern in-flow and out-flow, either into/out of a scaffold or chamber) and control of fluid selection through some valve operation was necessitated. Finally, all components were to be unified into an automation-capable software platform.

3D printing parameters

Eighteen parts were designed for the assembly of the TIPD, organized into part families in Tables 1–4, all of which were designed in Solid Works CAD/CAM (Dassault Systems, Waltham, MA). Before 3D printing, all part files were converted into stereolithography (.stl) file format from Solid Works, each of which is available for replicative printing in Supplementary Data S1. All parts were sliced and 3D printed using the fused filament fabrication (FFF) technique through ideaMaker Slicing Engine and Raise3D N2+ printer (Irvine, CA). PLA filament (1.75 mm diameter, Raise3D) was extruded through a 0.4 mm nozzle at 205°C onto a heated bed with a BuildTak surface (Maplewood, NJ) set to 65°C. All parts were printed using a raft to facilitate bed adhesion, with a 0.30 mm raft gap from each model. Parts were printed at a speed of 50 mm/s with three shells, variable infills at 45% or greater (tabularized below, based on part), and with support structures at 10% infill where any overhand angle greater that 40° received support. Approximate print times and estimated part masses presented in the Tables 1–4 are based on these slicing and printing parameters, however, parameters will likely vary depending on the printer and filament being used.

Machine design and assembly

CAD/CAM renderings of the TIPD assemblies are presented in Figure 1A and B. The TIPD was designed to include two peristaltic pumps, two 3-way valves, and to accommodate

Table 1. Part Family: Device Scaffold

Part name	*Thumbnail image (not to scale)*	*Quantity needed*	*Approximate print time*	*Estimated mass [g]*	*Notes*
Quarter Scaffold		4	9 h 45 min	57.1	1
Scaffold Side Post		2	3 h 32 min	19.2	None

Thumbnails and information relevant to the 3D printed components of the Quarter Scaffold Part Family, which provides the overall support to the device. *Note 1*: In-print support material recommended.

3D, three-dimensional.

Table 2. Part Family: Peristaltic Pump

Part name	*Thumbnail image (not to scale)*	*Quantity needed*	*Approximate print time*	*Estimated mass [g]*	*Notes*
Stepper Chassis		2	2 h 20 min	12.2	1
Stepper Fastener		2	30 min	3.9	2
Pump Carousel		2	1 h 50 min	6.5	2, 3, 4
Post Collar		10	1 h 10 min	3.0	3, 4
Carousel Cap		2	35 min	3.6	None
Carousel Stabilizer		2	1 h 40 min	6.4	1
Luer-Lok Collar		2	1 h 20 min	5.8	None

Thumbnails and information relevant to the 3D printed components of the Peristaltic Pump Part Family. *Note 1:* In-print support material recommended; *Note 2:* 100% infill density recommended; *Note 3:* High-quality print recommended; *Note 4:* Part sanding and chemical polishing recommended.

two styles of chambers. Figure 1C and D present the TIPDs after printing and assembling the requisite components using basic hardware. All through-holes and junctions have been designed to accommodate M3 machine screws (McMaster-Carr, Aurora, OH). Tubing, coupling, motors, and electronics are presented in detail in Supplementary Table S1. For ease of repeat assembly, the TIPD can be segmented into four-part families, which include the Device Scaffold subassembly, the Peristaltic Pump subassembly, the Valve Operation subassembly, and the Chamber Support subassembly.

The Device Scaffold subassembly provides structural support for the remaining three subassemblies. Table 1 presents the components necessary to create the Device Scaffold. Four Quarter Scaffold parts are organized such that a rectangular scaffold is made, occupying a footprint of 5.5″ (14.0 cm) wide by 5″ (12.7 cm) deep with a height of 8″ (20.3 cm). The Quarter Scaffold part has been designed with elongated through-holes allowing variable placement of the Pump and Valve subassemblies, designed to be affixed using M3 screws. Each Quarter Scaffold also possesses bores in which magnets

Table 3. Part Family: Valve Operation

Part name	*Thumbnail image (not to scale)*	*Quantity needed*	*Approximate print time*	*Estimated mass [g]*	*Notes*
Valve Chassis		2	1 h 40 min	9.8	1
Valve Rotator		2	20 min	0.9	1

Thumbnails and information relevant to the 3D printed components of the Valve Operation Part Family. *Note 1:* In-print support material recommended.

Table 4. Part Family: Chamber Support

Part name	*Thumbnail image (not to scale)*	*Quantity needed*	*Approximate print time*	*Estimated mass [g]*	*Notes*
Yaw Chassis Bracket		1	1 h 39 min	11.1	1
Servo Roll Chassis	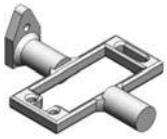	1	2 h 40 min	19.6	1
Roll Chassis Buckle		1	21 min	3.3	1
Servo Spacer		2	34 min	2.9	None
Top-Chamber Chassis		1	7 h 26 min	70.0	1
Side-Chamber Chassis		1	2 h 34 min	15.8	1
Cylindrical Chamber Cap		2	12 h 37 min	87.3	2, 3

Thumbnails and information relevant to the 3D printed components of the Chamber Support Part Family. *Note 1:* In-print support material recommended; *Note 2:* 100% infill density recommended; *Note 3:* High-quality print recommended.

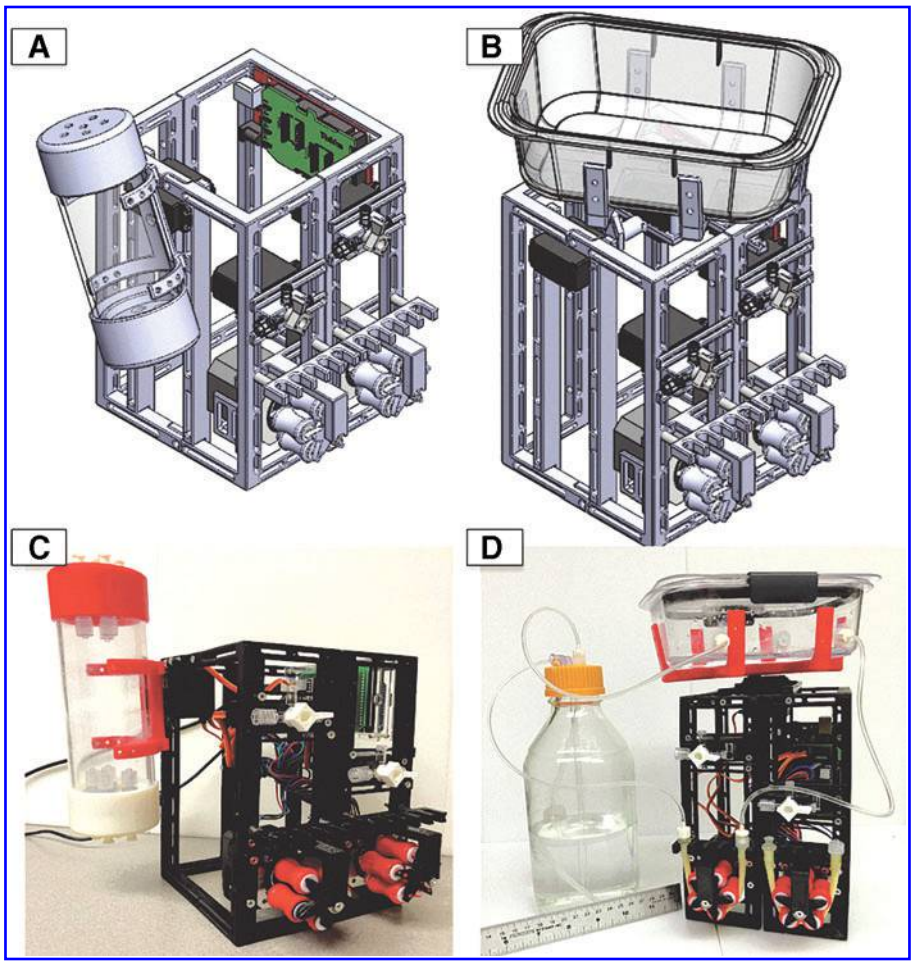

FIG. 1. (**A, B**) Solid Works CAD/CAM renderings of the TIPD with the *side-mount* and the *top-mount* chamber designs, respectively. (**C, D**) Designs after 3D printing and assembly of all components. For scale, a standard 1L glass Pyrex bottle is shown in **(D)**. 3D, three-dimensional; TIPD, tissue infusion/perfusion device.

can be press fit (optional). Figure 2 demonstrates the subassembly in isometric, top, and front views. Sixteen magnets can be seen in this exploded view from each of the four Quarter Scaffold parts of the subassembly. Near each magnet bore is a through-hole for permanent fixation through machine screw. Note that Figure 2 does not show the Scaffold Side Post; however, this structure is utilized to support a servomotor responsible for chamber motion, which is shown in the assemblies of Figure 1A and B.

The Peristaltic Pump subassembly creates the mechanism for driving fluid flow from a reservoir into the scaffold. Table 2 details the 3D printed part family for creating this subassembly, which consists of a combination of 3D printed parts as well as commercially available components. A NEMA 17 bipolar stepper motor (Stepper Online, Nanjing City, China) is used to generate the rotational movement of the pump. The Pump Carousel is designed to be press-fit onto the horn of the stepper motor, where a notch in the

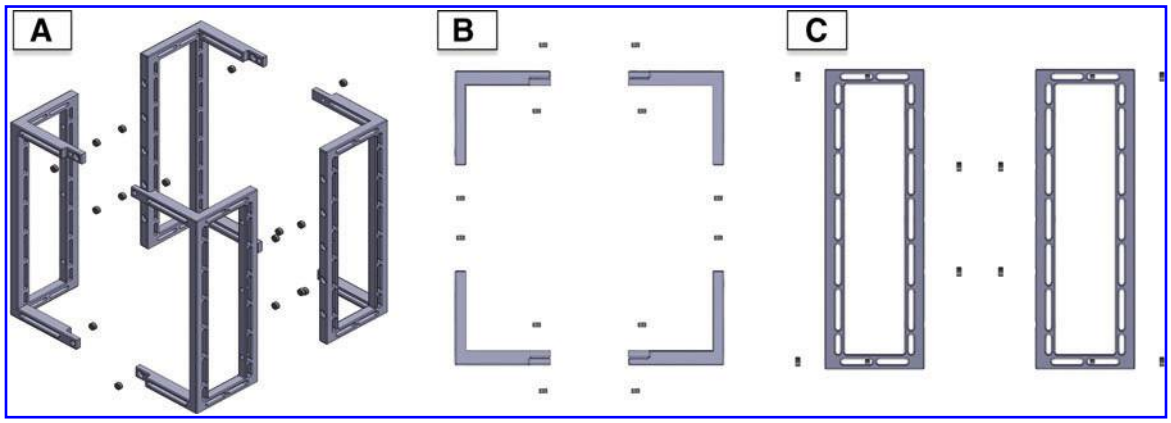

FIG. 2. (**A–C**) Exploded renderings of the Quarter Scaffold of the TIPD in isometric, *top*, and *front views*. In each image, sixteen 6×3 mm magnets are exploded from the Quarter Scaffolds, where four magnets per part are press-fit for ease of dis/assembly.

Pump Carousel will determine proper placement onto the motor. The Pump Carousel accommodates five Post Collars, which roll freely and create the peristaltic action when a tube is pulled taut against the faces of the Post Collars. In an effort to reduce friction during operation, Post Collars and the Pump Carousel were printed using the highest quality print setting available on the N2+ as definable in ideaMaker; the posts of the Pump Carousel, as well as the outer surface of the Post Collars, were sanded with fine-grit sandpaper and then were chemically polished using ethyl acetate (Millipore-Sigma, St. Louis, MO), smoothing the posts of the Pump Carousel as well as the Post Collar surfaces.

Additionally, an M5 unthreaded spacer (McMaster-Carr) inserts into each Post Collar, which further minimizes friction against the posts of the Pump Carousel during operation. Likewise, two M5 PTFE washers (McMaster-Carr) rest at the top and bottom of each Post Collar, separating it from the Carousel Cap and the base of the Pump Carousel. The Carousel Cap secures the Post Collars onto the Pump Carousel, and is assembled with a ball bearing separated by a 3 mm-long unthreaded spacer, holstered by the Carousel Stabilizer. Once all components within the subassembly are assembled, they are affixed to a Quarter Scaffold. Figure 3A presents these components in exploded view. Once the pump is assembled, the Stepper Fastener, Stepper Chassis, and the Carousel Stabilizer components are used to affix the stepper motor with the assembled carousel onto the Quarter Scaffold (refer to Fig. 1). The Luer-Lok Collar is then affixed to a Quarter Scaffold, resting atop the Carousel Stabilizer. A 10 cm tube with Luer-Lok couplers may then be wrapped around the assembled carousel, held in tension by the Luer-Lok Collar. The TIPD was designed to integrate two sets of this subassembly yielding independent peristaltic pumps capable of programmatically driving fluid at a controlled rate.

The Valve Operation subassembly is designed specifically for interfacing with a 4-Way Stopcock (Qosina, Ronkonkoma, NY; Part No. 88218). The 3D printed part family is presented in Table 3, and Figure 3B presents the exploded view of the subassembly. The Valve Chassis is responsible for holding the stopcock above the servomotor, and has been designed for adhesive fixation of an M3 hex nut, which stabilizes the stopcock when light pressure is applied from a thumbscrew. The Valve Rotator has been designed with a through-hole that seats concentrically with respect to the horn of a servomotor (DFRobot, Pudong, China) such that the Valve Rotator can be screwed directly into the servomotor. This minimizes the potential slippage of the Valve Rotator on the servomotor horn when turning the stopcock via servomotor control. For assembly onto a Quarter Scaffold, the servomotor with the affixed Valve Rotator is placed first, followed by the Valve Chassis. The top of the Valve Rotator interfaces directly with the bottom of the stopcock when seated within the Chassis.

The Chamber Support subassembly can be constructed in one of two ways: a hanging-mount design (Fig. 1A, C) or a top-mount design (Fig. 1B, D). Table 4 details the 3D printed components needed for each assembly. The hanging-mount design is constructed to hold a 2.25″-diameter tube (Supplementary Table S1), which is cut to a 4″ (10.2 cm) length in Figure 1 but can cut to an application-specific length. The side-mount design couples a single servomotor with the Side-Chamber Chassis and allows oscillatory movement between 0° and 180°. The top-mount design has been constructed for use with a commercially available 750-mL container (Rubbermaid), and integrates additional complexity into its assembly allowing for movement in the roll and yaw directions. Figure 3C–E present exploded views of the parts and hardware for creating the top-mount design. The Servo Roll Chassis (shown in Fig. 3D) accommodates a servomotor, governing the roll direction; this servomotor is horizontally mounted onto Scaffold Side Posts and then the opposing, cylindrical end of the Servo Roll Chassis is supported by mounting the subassembly shown in Figure 3C onto the top of the assembled Quarter Scaffolds. The Top-Chamber Chassis is secured into the servomotor using an M3 screw. The entire subassembly, including the 750-mL chamber, is shown in Figure 3F.

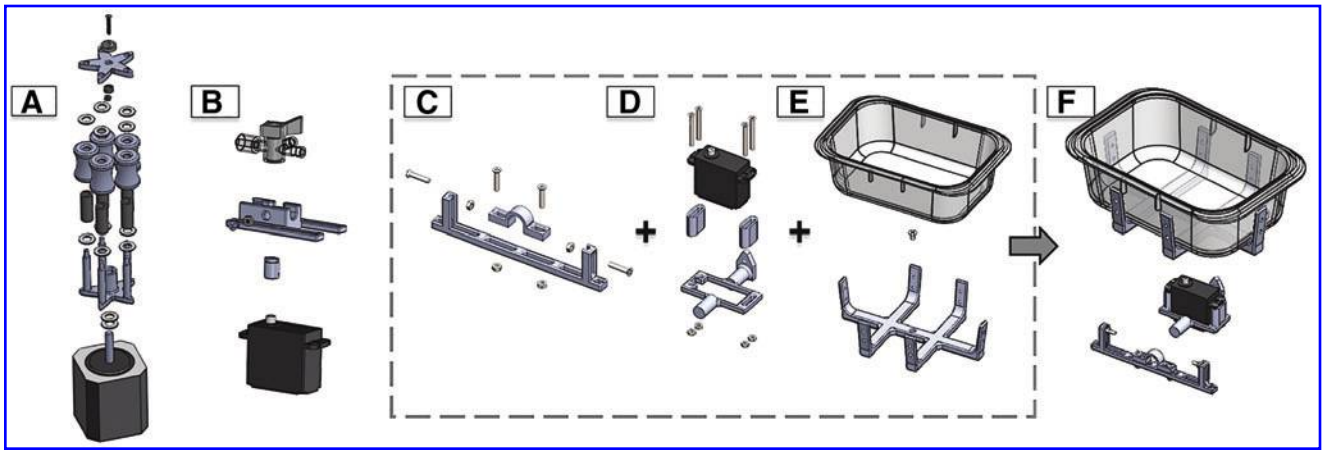

FIG. 3. **(A)** Exploded view of the Peristaltic Pump subassembly with a stepper motor at the base, driving the rotation of the pump once assembled. **(B)** Exploded view of the Valve Operation subassembly with a servomotor at the base, enabling valve selection within the 180° rotation range of the motor. **(C–E)** Exploded views of the *top-mount* chamber assembly. **(F)** The resulting subassembly of the *top-mount* chamber design.

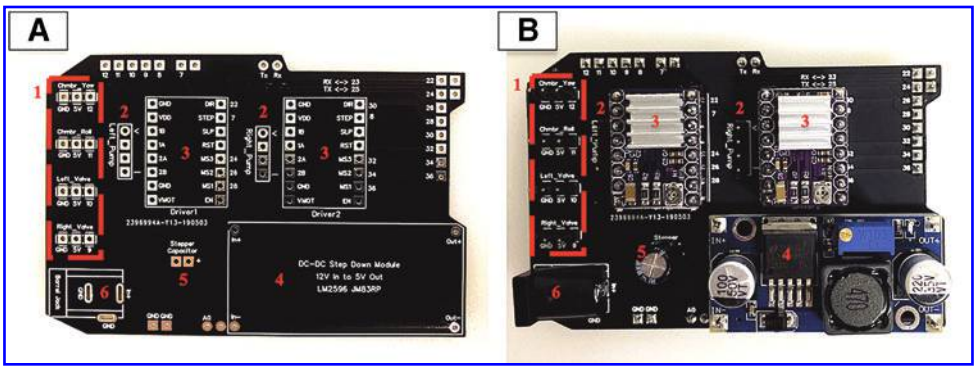

FIG. 4. **(A, B)** The nonpopulated PCB and PCB after soldering the requisite components, respectively. The six points of interest called out in the images denote the various pinouts, components, and modules necessary for controlling the device through Arduino-enabled microcontroller. PCB, printed circuit board.

Circuitry, electronics, and programmatic control

Logic-based control of the TIPDs electronic components is based around an Arduino Mega2650 microcontroller (Ivrea, Italy) and a custom-printed circuit board (PCB), which forms an Arduino shield once assembled. Layout of the PCB was designed in EasyEDA and fabricated by JLC PCB (Shenzhen, China). A zipped folder containing the respective GERBER files is provided in Supplementary Data S2, which can be uploaded directly into the JLC PCB portal. Figure 4A and B show the unpopulated PCB and the PCB after soldering all components into place, respectively. From Figure 4, numeric labels 1–6 indicate Components/Component Sets: Component Set 1 denotes four sets of male pinouts for the servomotors (chamber movement and valve operation). Component Set 2 denotes two sets of male pinouts for the stepper motors (peristaltic pumps). Component Set 3 denotes two sets of DRV8825 Stepper Motor Drivers (Pololu, Las Vegas, NV), which are responsible for converting the logic received from the microcontroller into the appropriate rotational pump speed. Component 4 denotes a DC-DC step-down module that is adjusted to 5 V output from 12 V input, which powers both the stepper and servo motors. Component 5 is a 100 μF capacitor, and is used for smoothing the current of the stepper motors on startup. Finally, Component 6 denotes a 2.1 mm barrel jack, which accommodates a 12 V 5A power supply that is responsible for powering the system independent of the microcontroller.

The Arduino integrated development environment (IDE) was downloaded, which includes the requisite drivers for running the microcontroller. All coding for the TIPD was done through virtual instrument (VI) in LabVIEW 2018 (National Instruments, Austin, TX) with the Digilent LINX package add-on from the Virtual instrument Package Manager (JKI, Lafayette, CA). The LINX prebuilt hex was installed onto the Arduino before operation. Main and sub-VIs were saved as an Executable (.exe) file extension and are available in Supplementary Data S3. Note, for running the Executable, NI-VISA RunTime Engine 18.5 must be installed such that LabVIEW is able to recognize use of a COM port by the microcontroller. Additionally, either the full version of LabVIEW or LabVIEW SP1 RunTime 19 must be installed. Windows OS was used throughout.

Proof of concept through infusion and perfusion decellularization

Porcine skeletal quadriceps muscle from male Yorkshire pigs was obtained immediately after sacrifice, and was stored at −80°C before decellularization. Muscle was thawed and cut into contiguous segments of 1.25 ± 0.05 g after which an 18G Precision Glide sharp-tip needle (BD, Franklin Lakes, NJ) was inserted into the muscle such that the needle opened at approximately the centroid of the segment.

Rodent kidneys from recently deceased Lewis rats were obtained, where the vascular and ureter pedicle were cannulated using 20G Introcan IV catheters for the renal artery and ureter and a 24G Introcan IV catheter (B. Braun, Bethlehem, PA) for the renal vein. The kidney was flushed with 10 mL heparinized saline before decellularization. For infusion and perfusion decellularization, 100 mL 0.3% or 1% sodium dodecyl sulfate (SDS; Millipore-Sigma) was pumped for ∼20 h, where the SDS was recirculated after tissue contact (0.3% was only used for infusion decellularization). Next, 1000 mL deionized (DI) water was pumped through the tissue and was not recirculated. To further ensure clearance of the SDS, 100 mL 1% Triton X-100 (Millipore-Sigma) was pumped and recirculated through the tissue for 20 h, followed by an additional 1000 mL DI water (nonrecirculated). The pump was set to 1/8-step for all processes. Separately, muscle was decellularized in a spinner flask following previously established protocols.[21,22] Briefly, the spinner flask was set to 400RPM and a ratio of 1:10 muscle mass to solution volume was exposed to 1% SDS for 3 days. Residual SDS was removed using eight exchanges of DI water, followed by an additional exposure of 1% Triton X-100 overnight. Finally, the muscle was exposed to eight additional exchanges of DI water.

Hematoxylin and eosin staining

After decellularization, soft tissues were fixed in 10% neutral buffer formalin (Fisher Scientific, Waltham, MA), paraffin-embedded, and mounted in 5 μm sections on polarized glass slides. Hematoxylin and Eosin (H&E) staining was performed by removing paraffin at 60°C for 60 min and then rehydrating sections in serial washes of decreasing ethanol concentrations. Wiegert's H&E was applied as per manufacturer's instruction (Millipore-Sigma). Sections were then dehydrated and mounted with slide glass. A Keyence BZ-X was used for all histological imaging.

DNA quantification of muscle

Muscle was frozen to −80°C and then freeze dried (Labconco FreezeZone 2.5, Kansas City, MO). Dry samples of 25 ± 5 mg were digested in proteinase-k and purified following the manufacturer's instructions (QIAamp; Qiagen,

Germantown, MD). DNA was quantified using the QUANT-it PicoGreen dsDNA Kit as per the manufacturer's instructions (Fisher Scientific).

Statistical analyses

JMP Pro 14 was used for statistical analyses. DNA results were evaluated using a one-way analysis of variance with Tukey–Kramer *post hoc* after testing for normalcy of residuals through Shapiro–Wilk *W*-test and homoscedasticity through Levene's tests. Statistical significance was defined as $p < 0.05$.

Results

LabVIEW VI and automation capabilities

Figure 5A and B display the graphical user interface (GUI) when running the VI in Control and Automation modes, respectively. Nineteen points of interest are displayed in the Figure 5: (1) denotes the Communication Port ''COM#'' tethered to the PCB-shielded microcontroller, to be defined before running the VI; (2) displays the current time and date; (3) displays the total runtime of the VI; (4) is a notifier that changes based on operating state of the TIPD; (5) displays a resettable clock; (6) denotes a set of indicators that control the movement of the chamber, being either yaw movement if the top-mount chamber is affixed, or the oscillatory movement if the side-mount chamber is affixed; (7) denotes a set of indicators that control the roll movement of the top-mount chamber only (*note:* the chamber control values dictate pulse widths sent from the microcontroller to the servomotor and are arbitrary with respect to the physical orientation of the servomotor horn); (8) indicates communication to the microcontroller when illuminated green; (9) displays three selectable panels being the Main Control panel (Fig. 5A), the Automation panel (Fig. 5B), and the Settings panel, which allows additional user customization of servomotor boundaries; (10) denotes a push button to stop one or both pumps if running; (11) displays an indicator light, which illuminates when the pump is active, along with a scale bar ranging from Off to Full that determines the spin rate of the pump; (12) denotes a switch that reverses the pump direction; (13) denotes controls for the 3-way valve, where ''Timed'' is a function controlling oscillation between the top or side port being open; (14) denotes another set of the controls and indicators explained in (11–13) for the opposing pump; (15) denotes the file selection window for running an automation protocol from a comma-separated (.csv) file; an Excel template for building custom automation protocols has been provided in Supplementary Data S4; (16) displays the Initiate Automation buttons, which will only become active when a protocol is defined in the selection window and the notifier as discussed in (4) is updated with the current step, step time, and the overall protocol time as shown; (17) displays the Abort Automation button, which will only become active when a protocol is running; (18) displays a table of the entire protocol once initiated; finally, (19) like (9) presents the selection tab but with the Automation panel active. Through manual control or through automation, the TIPD is capable of controlling fluid flow spanning the six-step motor range. Figure 6A and B present the flow velocity by the step size and the flow velocity by the revolutions per minute and their fitted curves, respectively. As shown, the pumps are capable of achieving flow rate of up to 1.25 mL/s (4.50 L/h). Intermittent flow rates can be achieved by utilizing the ''Active''/''Inactive'' setting in the VI.

On harvest, vascular access to some tissue types cannot be established and hence an infusion method may be utilized to similarly replicate perfusion decellularization. Figure 6C–E display setup for skeletal muscle infusion, infusion decellularization inside the side-mount chamber, and the resulting scaffold, respectively. A time lapse of the 20-h SDS portion of the infusion decellularization as well as a video of dual muscle infusion with activated chamber oscillation can be viewed in Supplementary Video S1 and S2, respectively. The H&E image in Figure 6F shows native porcine skeletal

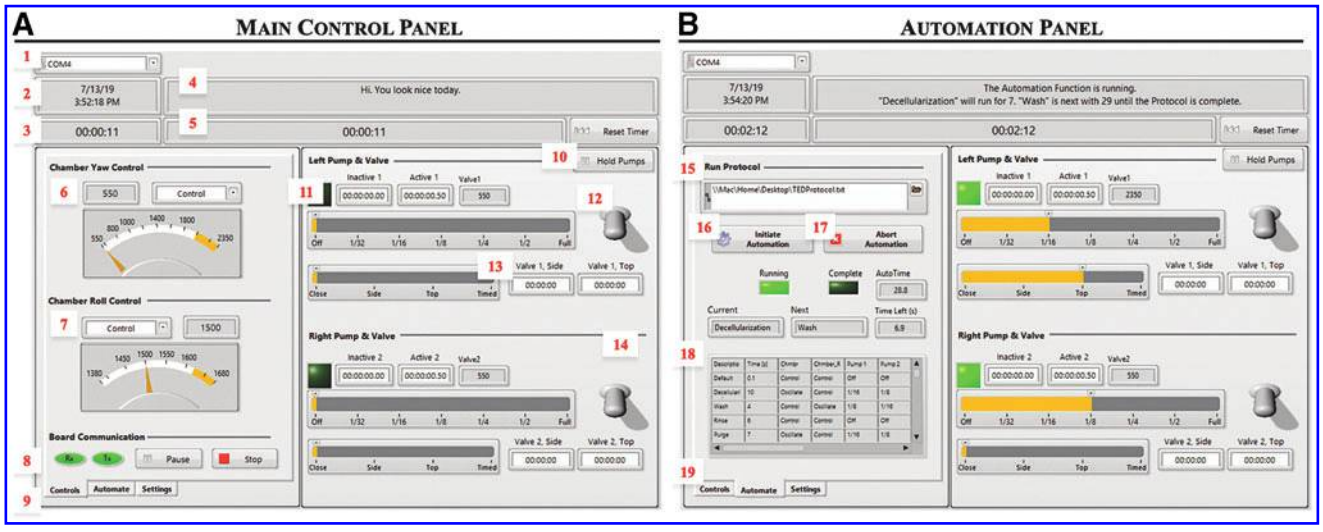

FIG. 5. **(A)** GUI of the LabVIEW VI written to control the TIPD in the Control panel. **(B)** GUI in the Automation panel, where a protocol for the automation of a process has been selected and initiated as shown by the Notifier (Callout 4) and the Automation Matrix (Callout 18). GUI, graphical user interface.

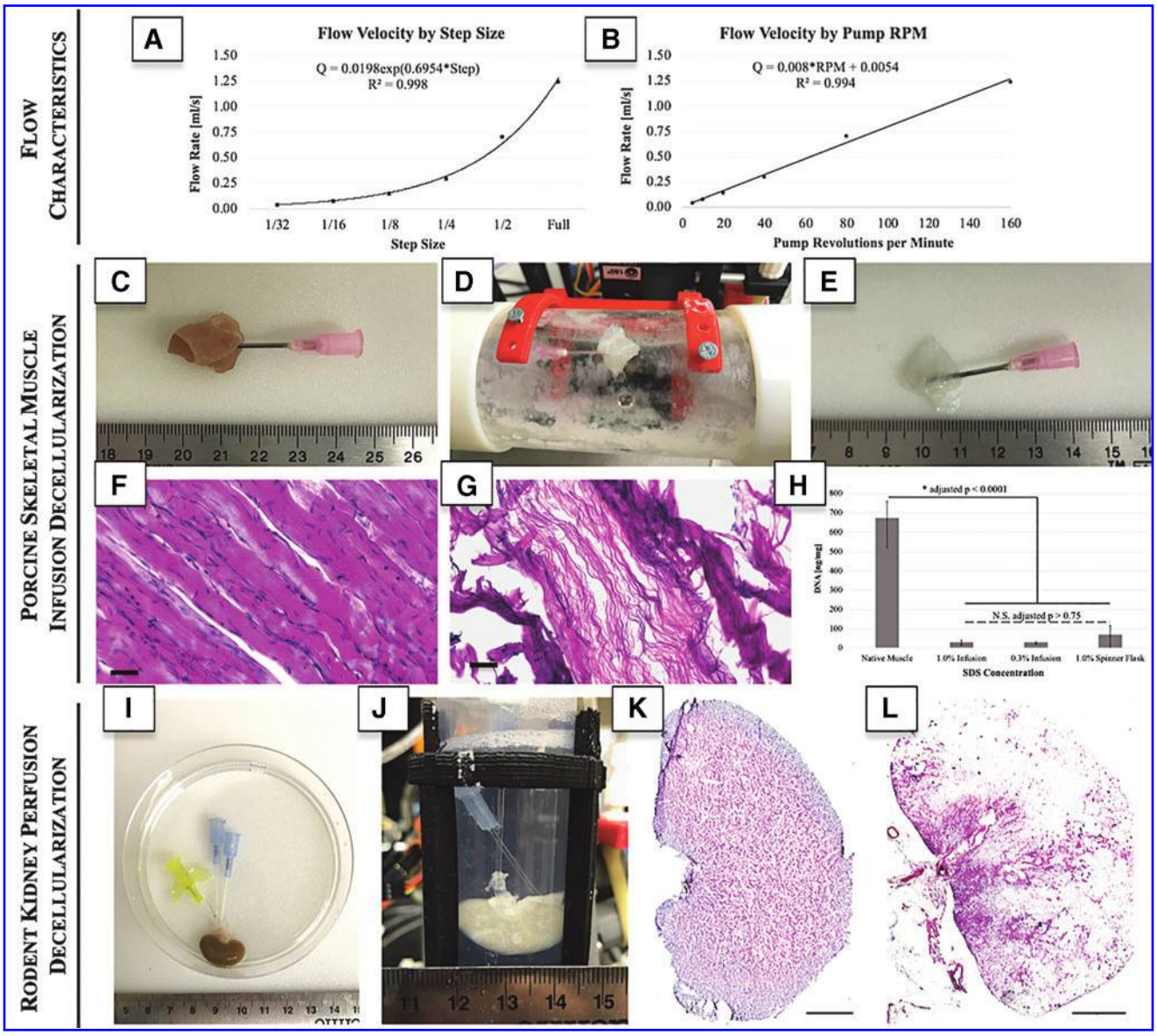

FIG. 6. **(A, B)** Fluid velocity characteristics of the over the range of peristaltic pumps governed by the step size of the motor; exponential and linear equations are shown for predicting flow rates at intermittent pump steps. **(C–E)** Steps of infusion decellularization of porcine skeletal muscle where a needle is inserted into the muscle body, the needle junction is affixed within the chamber, and after SDS-based infusion decellularization, the resulting muscle ECM becomes translucent. **(F–H)** H&E staining of native porcine muscle, confirmation of decellularization by H&E staining (scale bars: 50 μm), and DNA quantification, respectively; compared with native porcine skeletal muscle, all decellularization processes resulted in significant DNA reduction, however, infusion decellularization was able to achieve this result in half the time and at a lower concentration of SDS. **(I, J)** SDS-based perfusion decellularization of a rodent kidney where the vein, artery, and ureter were cannulated, the artery affixed to receive inflow with the resulting translucent scaffold. **(K, L)** H&E staining of native rodent kidney presenting significant nuclei about the periphery and H&E staining devoid of nuclear material after perfusion decellularization (scale bars: 5 mm). ECM, extracellular matrix; H&E, Hematoxylin and Eosin; SDS, sodium dodecyl sulfate.

muscle and Figure 6G presents H&E of the fibrous ultrastructure lacking nuclei after decellularization, which is confirmed by DNA quantification (Fig. 6H). As shown, significant reduction of DNA was achieved in all decellularization processes with respect to native porcine skeletal muscle ($p < 0.001$). No significant difference in DNA content was found when comparing 20-h 0.3% or 1% SDS infusion processes against the 72-h 1% SDS spinner flask process (adjusted $p > 0.750$ for each comparison). Decellularization of vascularized composite tissues can be achieved using perfusion in the same system, although requires cannulation of at least one vessel for successful perfusion. Figure 6I and J display a rodent kidney cannulated IV catheters, where the artery is affixed to a Luer-Lok junction for establishing fluid flow and subsequent decellularization. Figure 6K displays H&E of a native rodent

kidney, presenting nuclei prominently about the periphery. Figure 6L displays H&E of the kidney after decellularization showing preservation of the ultrastructure nearest to the pedicle and lacking visible nuclei.

Discussion

A TIPD capable of automated decellularization, which possesses the ability for a user to easily alter input parameters in real-time, has been described. Consistent with the open-source initiative,[23] the TIPD has been designed as an OSH platform using components designed for replication through 3D printing (Supplementary Data S1) in conjunction with commercially available hardware (Supplementary Table S1). Two types of chambers are designed in this study, and although the cylindrical chamber is better lent to being constructed with 3D printed components, its leak-proof construction is nuanced. Although leak proofing was achieved using the Raise3D printer, this required 100% infill and the highest quality print setting offered on the printer used. Since leak proofing is an essential aspect of any fluidic devices, a commercially available and leak-proof component is offered here to avoid the potential difficulties when using FFF-printed components given the resolution and fusion variability between printers and filaments.

Use of either chamber over the other for any given process or tissue type is discretionary since the critical component is the entrance and exit of fluid and not the vessel in which it is housed. Rotation of the two chamber types was integrated as a feature for the user to better control the posture of a tissue within a chamber. This is particularly relevant for preventing kinks or twists in tissue pedicles, which can induce thrombosis during perfusion.[24] If a user's application does not require such motion, these components can be subtracted from the system with no adverse effect on the function of the electronics or software. Driving these servomotors, the valve servomotors, and the stepper motors governing the peristaltic pumps, is an Arduino microcontroller, which was selected because it is an open-source electronics platform based on an IDE that allows for control of a myriad of devices capable of interacting with the external environment and shares a large developer community that has written, tested, and published functional code.[25,26] Although an Executable (.exe) has been formed from a LabVIEW VI file, the compilation of code and communication to the hardware within the system is not limited to the provided VI alone. The VI that is provided, however, leverages integration of the components into a single GUI and transfers the processing from the microcontroller to a computer, which is more ideal for accomplishing nonrepetitive tasks relative to a microcontroller.

Implementation of a peristaltic pump has been key for both infusion[27] and perfusion tissue engineering bioreactors.[28] The TIPD is configurable such that either infusion directly into a tissue or perfusion of tissue vasculature can be achieved as shown through the decellularization of porcine skeletal muscle and a rodent kidney, respectively. Using the infusion technique, 48 h less SDS exposure time was utilized to achieve similar residual DNA results, which could also be achieved with a lesser concentration of SDS. This may be of importance in the context of matrix preservation due to the cytotoxic nature of SDS,[29] and its ability to denature collagenous fibrils of ECM in cases of prolonged exposure when assessed in decellularizing urinary bladder and tendon.[30] Since the muscle was frozen before decellularization (both spinner flask and infusion), the freeze/thaw cycle likely played a role in enhancing the decellularization processes at least somewhat; such mechanical disruption has been shown to assist decellularization when implemented repeatedly, although complete decellularization is only obtained with additional steps like surfactant exposure.[31–33] In these instances of infusion decellularization of muscle tissue, the chamber was not filled with fluid to appreciate the infusion process and compare it to spinner flask decellularization. It is conceivable that infusion decellularization coupled with a fluid-filled chamber may facilitate increasingly rapid decellularization; this, however, requires further investigation.

Perfusion through the renal artery of a rodent kidney was achieved to show proof of concept for perfusion decellularization, where the resulting scaffold and H&E staining resulted in a translucent scaffold. Conceptually, the method of arterial cannulation and perfusion-based flow can be achieved in any vascular structure able to accommodate a port, but doing so in this specific system requires further investigation. Additionally, understanding the effects that fluidic shear imposes on the integrity or directionality of residual fiber alignment within a scaffold warrants additional investigation. Integration of infusion and perfusion capabilities into a single platform allows programmatic decellularization of tissue and organ types beyond what has been explored here. Decellularization of many tissue types do not establish vascular access, and therefore use spinner flask-based processes; such tissue types have included tendon,[34] peripheral nerve,[35] or cartilage,[36] where an infusion process similar to what was done in this study with muscle segments could be used. While muscle was infused with an 18G needle punctured into the centroid of the scaffold, optimization to facilitate decellularization of additional tissue types would likely require adjusting needle size as the tissue segments change in size. Furthermore, the addition of multiple points of entry would likely enhance infusion decellularization. Utilizing the same device, perfusion decellularization of solid organs through pedicle access is achievable, although the device would likely be better suited to have anatomically relevant outflows present (i.e., for the kidney, inflow into the artery, and independent outflows from the vein and ureter). This could allow more direct control over the intrascaffold pressure, and speculatively, may better maintain the scaffold architecture if drawing fluid from the outflow(s) using one or a series of peristaltic pumps.

While this innovation is promising, there are several limitations with the platform at hand. Additional complexity could be integrated into the device that more accurately controls flow rates or intrascaffold pressures, which may increase the efficacy of decellularization and overall preservation of the vasculature network embedded within the matrix.[37] Notably, it has been shown that intrascaffold pressures better dictate successes in recellularization relative to constant flow velocities that do not adjust for pressure.[38] Cold-perfusion decellularization of pancreatic tissue has shown improved retention of the vascular network relative to its ambient temperature counterpart.[39] Modifying the

device to include a cooling element within the chamber may function to achieve similar results, or alternatively the unit is of an appropriate footprint to fit inside a standard laboratory refrigerator. A paramount challenge in tissue engineering has been the development of a single, modular system that allows the versatility to decellularize tissues in the same device in which they will be recellularized, tested, and subsequently transported for providing a functional tissue-engineered therapy at the point of care.[40] To do so, the unit, as it stands, will require modifications in terms of additional fluid-handling capabilities, on-board monitoring of relevant quality characteristics, and preimplantation metrics able to ensure that a scaffold is suitable for *in vivo* use. Additionally, the scale of this prototype as designed is best suited for applications in small organ and tissue decellularization, and is therefore ill-suited for large animal/adult human organ engineering at present. This can largely be remedied by the reconstruction of the chambers to accommodate larger volumes as the pumps are able to achieve physiologically relevant flow velocities for larger organs. Despite its limitations, the platform described in this study is suitable for creating repeatable decellularization processes and is readily expandable with the litany of components that are commercially available for significantly expanding the current capabilities of the device.

Conclusion

The TIPD designed is a compact, integrated system capable of automated decellularization of multiple tissue types through fluid infusion or perfusion. The TIPD has been created with OSH and using 3D printed components that are replaceable if damaged and easily replicated across laboratories. The code governing the TIPD allows a user to define an automation protocol, creating an opportunity to greatly enhance the repeatability between instances of decellularization with a program capable of precisely specifying when solution changes are to occur in a given process. The system has been designed with the intention of increasing reproducibility and repeatability throughout decellularization and ideally can be implemented readily across many niches of tissue engineering.

Acknowledgments

The authors would like to thank Brian Moyer, Asim Ejaz, Andrea Schilling, Lauren Kokai, William Federspiel, Ryan Orizondo, and Brian Frankowski for their input and assistance with the approach, design, assembly, coding, and operation of the TIPD.

Disclosure Statement

No competing financial interests exist.

Funding Information

No funding was received for this work.

Supplementary Material

Supplementary Data S1
Supplementary Data S2
Supplementary Data S3
Supplementary Data S4
Supplementary Table S1
Supplementary Video S1

References

1. Parmaksiz, M., Dogan, A., Odabas, S., *et al.* Clinical applications of decellularized extracellular matrices for tissue engineering and regenerative medicine. Biomed Mater **11,** 022003, 2016.
2. Shankaran, V., Weber, D.J., Reed 2nd, R.L., *et al.* A review of available prosthetics for ventral hernia repair. Ann Surg **253,** 16, 2011.
3. Primus, F.E., and Harris, H.W. A critical review of biologic mesh use in ventral hernia repairs under contaminated conditions. Hernia **17,** 21, 2013.
4. Sbitany, H. and Serletti, J.M. Acellular dermis-assisted prosthetic breast reconstruction: a systematic and critical review of efficacy and associated morbidity. Plast Reconstr Surg **128,** 1162, 2011.
5. Becker, S., Saint-Cyr. M., Wong, C., *et al.* AlloDerm versus DermaMatrix in immediate expander-based breast reconstruction: a preliminary comparison of complication profiles and material compliance. Plast Reconstr Surg **123,** 1, 2009.
6. Kokai, L.E., Schilling, B.K., Chnari, E., *et al.* Injectable allograft adipose matrix supports adipogenic tissue remodeling in the nude mouse and human. Plast Reconstr Surg **143,** 299e, 2019.
7. Grover, V., Kapoor, A., Malhotra, R., *et al.* Bone allografts: a review of safety and efficacy. Indian J Dent Res **22,** 496, 2011.
8. Shehadi, J.A., and Elzein, S.M. Review of commercially available demineralized bone matrix products for spinal fusions: A selection paradigm. Surg Neurol **8,** 203, 2017.
9. Krych, A.J., Jackson, J.D., Hoskin, T.L., *et al.* A meta-analysis of patellar tendon autograft versus patellar tendon allograft in anterior cruciate ligament reconstruction. Arthroscopy **24,** 292, 2008.
10. Snyder, R.J. Treatment of nonhealing ulcers with allografts. Clin Dermatol **23,** 388, 2005.
11. Sheikh, E.S., Sheikh, E.S., and Fetterolf, D.E. Use of dehydrated human amniotic membrane allografts to promote healing in patients with refractory non healing wounds. Int Wound J **11,** 711, 2014.
12. Porzionato, A., Stocco, E., Barbon, S., *et al.* Tissue-Engineered Grafts from Human Decellularized Extracellular Matrices: A Systematic Review and Future Perspectives. Int J Mol Sci **18,** E4117, 2018.
13. Robertson, M.J., Dries-Devlin, J.L., Kren, S.M., *et al.* Optimizing recellularization of whole decellularized heart extracellular matrix. PLoS One **9,** e90406, 2014.
14. Lu, T.Y., Lin, B., Kim, J., *et al.* Repopulation of decellularized mouse heart with human induced pluripotent stem cell-derived cardiovascular progenitor cells. Nat Commun **4,** 2307, 2013.
15. Gilpin, S.E., Ren, X., Okamoto, T., *et al.* Enhanced lung epithelial specification of human induced pluripotent stem cells on decellularized lung matrix. Ann Thorac Surg **98,** 1721, 2014.
16. Poornejad, N., Buckmiller, E., Schaumann, L., *et al.* Re-epithelialization of whole porcine kidneys with renal epithelial cells. J Tissue Eng **8,** 2041731417718809, 2017.
17. Duisit, J., Orlando, G., Debluts, D., *et al.* Decellularization of the Porcine Ear Generates a Biocompatible, Non-immunogenic Extracellular Matrix Platform for Face Subunit Bioengineering. Ann Surg **267,** 1191, 2018.

18. Gilpin, A., and Yang, Y. Decellularization Strategies for Regenerative Medicine: From Processing Techniques to Applications. Biomed Res Int **2017,** 9831534, 2017.
19. Guyette, J.P., Gilpin, S.E., Charest, J.M., *et al.* Perfusion decellularization of whole organs. Nat Protoc **9,** 1451, 2014.
20. Price, A.P., Godin, L.M, Domek, A., *et al.* Automated decellularization of intact, human-sized lungs for tissue engineering. Tissue Eng Part C Methods **21,** 94, 2015.
21. DeQuach, J.A., Lin, J.E., Cam, C., *et al.* Injectable skeletal muscle matrix hydrogel promotes neovascularization and muscle cell infiltration in a hindlimb ischemia model. Eur Cell Mater **23,** 400, 2012.
22. DeQuach, J.A., Mezzano, V., Miglani, A., *et al.* Simple and high yielding method for preparing tissue specific extracellular matrix coatings for cell culture. PLoS One **5,** e13039, 2010.
23. Pearce, J.M. Materials science. Building research equipment with free, open-source hardware. Science **337,** 1301, 2012.
24. Zhan, W., Marre, D., Mitchell, G.M., *et al.* Tissue engineering by intrinsic vascularization in an *in vivo* tissue engineering chamber. J Vis Exp **e54099,** 1, 2016.
25. Margolis, M. Arduino Cookbook: Recipes to Begin, Expand, and Enhance Your Projects. Sebastopol, CA: O'Reilly Media, Inc., 2011.
26. Oxer, J. and Blemings, H. Practical Arduino: Cool Projects for Open Source Hardware. Norwich, NY: Apress, 2011.
27. Kasukonis, B., Kim, J., Brown, L., *et al.* Codelivery of infusion decellularized skeletal muscle with minced muscle autografts improved recovery from volumetric muscle loss injury in a rat model. Tissue Eng Part A **22,** 1151, 2016.
28. Scarritt, M.E., Pashos, N.C., and Bunnell, B.A. A review of cellularization strategies for tissue engineering of whole organs. Front Bioeng Biotechnol **3,** 43, 2015.
29. Caamano, S., Shiori, A., Strauss, S.H., *et al.* Does sodium dodecyl sulfate wash out of detergent-treated bovine pericardium at cytotoxic concentrations? J Heart Valve Dis **18,** 101, 2009.
30. Hwang, J., San, B.H., Turner, N.J., *et al.* Molecular assessment of collagen denaturation in decellularized tissues using a collagen hybridizing peptide. Acta Biomater **53,** 268, 2017.
31. Burk, J., Erbe, I., Berner, D., *et al.* Freeze-thaw cycles enhance decellularization of large tendons. Tissue Eng Part C Methods **20,** 276, 2014.
32. Roth, S.P., Glauche, S.M., Plenge, A., *et al.* Automated freeze-thaw cycles for decellularization of tendon tissue - a pilot study. BMC Biotechnol **17,** 13, 2017.
33. Gillies, A.R., Smith, L.R., Lieber, R.L., *et al.* Method for decellularizing skeletal muscle without detergents or proteolytic enzymes. Tissue Eng Part C Methods **17,** 383, 2011.
34. Lovati, A.B., Bottagisio, M., and Moretti, M. Decellularized and engineered tendons as biological substitutes: A critical review. Stem Cells Int **2016,** 7276150, 2016.
35. Choi, J., Kim, J.H., Jang, J.W., *et al*. Decellularized sciatic nerve matrix as a biodegradable conduit for peripheral nerve regeneration. Neural Regen Res **13,** 1796, 2018.
36. Duisit, J., Amiel, H., Wuthrich, T., *et al.* Perfusion-decellularization of human ear grafts enables ECM-based scaffolds for auricular vascularized composite tissue engineering. Acta Biomater **73**, 339, 2018.
37. Momtahan, N., Poornejad, N., Struk, J.A., *et al.* Automation of pressure control improves whole porcine heart decellularization. Tissue Eng Part C Methods **21,** 1148, 2015.
38. Lichtenberg, A., Cebotari, S., Tudorache, I., *et al.* Flow-dependent re-endothelialization of tissue-engineered heart valves. J Heart Valve Dis **15,** 287, 2006.
39. Elebring, E., Kuna, V.K., Kvarnstrom, N., *et al.* Cold-perfusion decellularization of whole-organ porcine pancreas supports human fetal pancreatic cell attachment and expression of endocrine and exocrine markers. J Tissue Eng **8,** 2041731417738145, 2017.
40. Martin, I., Simmons, P.J., and Williams, D.F. Manufacturing challenges in regenerative medicine. Sci Transl Med **6,** 232fs216, 2014.

Address correspondence to:
Kacey G. Marra, PhD
Department of Plastic Surgery
University of Pittsburgh
203 Lothrop St. Biomedical Science Tower E1655
Pittsburgh, PA 15213

E-mail: marrak@upmc.edu

Received: August 8, 2019
Accepted: October 15, 2019
Online Publication Date: November 20, 2019